On the relative abundance of LiH and LiH⁺ molecules in the early universe: new results from quantum reactions

Stefano Bovino, Mario Tacconi, Franco A. Gianturco

Department of Chemistry and CNISM, the University of Rome "Sapienza", P.le A. Moro 5, 00185 Roma, Italy

Daniele Galli, Francesco Palla

INAF-Osservatorio Astrofisico di Arcetri, Largo E. Fermi 5, 50125 Firenze, Italy

fa.gianturco@caspur.it

ABSTRACT

The relative efficiencies of the chemical pathways that can lead to the destruction of LiH and LiH⁺ molecules, conjectured to be present in the primordial gas and to control molecular cooling processes in the gravitational collapse of the post-recombination era, are revisited by using accurate quantum calculations for the several reactions involved. The new rates are employed to survey the behavior of the relative abundance of these molecules at redshifts of interest for early universe conditions. We find significant differences with respect to previous calculations, the present ones yielding LIH abundances higher than LiH⁺ at all redshifts.

1. Introduction

The suggestion that chemical processes involving lithium could play a role in the evolution of the early universe in the post-recombination era has been put forward several years ago (Lepp & Shull 1983; Stancil et al. 1996, hereafter SLD96; Galli & Palla 1998; hereafter GP98), starting from the consideration that Li is produced a few minutes after the Big Bang and the formation of other light atoms like H, D and He (Wagoner et al. 1967, Peebles 1993). The fractional abundances of these elements are sensitive to the baryon density of the universe and set constraints on its actual value (Cyburt et al. 2008). As the universe expanded, its radiation temperature decreased and the atomic ions originating from the above elements gave rise to neutral atoms by recombination with electrons, thus initiating the formation of molecular species by radiative association: H₂, HD and LiH. The latter molecule, because of its large dipole moment and low ionization potential, may induce spatial and/or spectral distortions in the cosmic background radiation (CBR), as originally suggested by Dubrovich (1993) and as experimentally surmised by the pionering work of Maoli et al. (1994). Eventually, during the gravitational collapse leading to the formation of the first stars,

the low excitation threshold and the efficient radiative decay along the rotovibrational manifold are additional properties that could favor the role of LiH and LiH⁺ as molecular coolants of the primordial gas (Bougleux & Galli 1997, hereafter BG97). The nonequilibrium level population in the presence of a different gas and radiation temperature may have a possible signature in protogalactic clouds, imprinting small fluctuations in the CBR spectrum (Schleicher et al. 2008), as we shall further discuss in our conclusions.

The chemistry of Li in the early universe has been discussed in the past, reaching contrasting conclusions (see e.g., SLD96; BG97; GP98; Vonlanthen et al. 2009). Of critical relevance, is the uncertainty in the knowledge of reliable reaction rates for the destruction of LiH and LiH⁺ molecules via strongly exothermic reactions without entrance barriers:

$$LiH + H \rightarrow Li + H_2,$$
 (1)

$$LiH + H^+ \to Li + H_2^+, \tag{2}$$

and

$$LiH^{+} + H \rightarrow Li^{+} + H_{2}. \tag{3}$$

Therefore, it is an accurate knowledge of the reaction rates for the above processes, at low redshift values, that can ultimately tell us what the end-role of the LiH/LiH⁺ systems could be as efficient coolants under early universe conditions. The task of the present work is to show that the reaction rates recently determined from fully ab-initio quantum methods (Bovino et al. 2009, 2010a, 2010b), which also employ accurate interaction forces between partners, have a significant impact on the evolution of LiH and LiH⁺ during the post-recombination era of the early universe. We shall further show that a more realistic computational description of the rates for a neutralization process

$$LiH^+ + e^- \rightarrow Li + H$$
 (4)

could substantially change the relative abundance of the ionic molecular species.

This paper is organized as follows: the details of the quantum methods for the new chemical reaction rates are given in Section 2, while Section 3 reports the list of considered reactions and describes the equations controlling the evolution of the gas temperature. In Section 4 we present the fractional abundances and an analysis of their behavior, while Section 5 summarizes our present conclusions.

2. The quantum reactive calculations

The study of the chemical evolution of the main species of the primordial gas requires accurate rate coefficients for the most important destruction reactions. In previous works, the Langevin approximation for barrierless reactions has been the main method used to obtain the rate coefficients for those reactions. In the last decade, with the developing of more realistic methods for reaction

processes, a great deal of work has been done to study reactions (1), (2) and (3). For instance, time-dependent (Bulut et al. 2008, Defazio et al. 2005) and quasi-classical trajectory (Pino et al. 2008, Dunne et al. 2001) calculations have been reported, and some of the calculated rates have been included in the abundance calculations of Lepp et. al. (2002). However, most of these calculations are restricted to a narrow range of energies or are limited to the high energy regime. Therefore, the main improvement of the present calculations has been the use of new, very accurate, potential energy surfaces (Martinazzo et al. 2003a, 2003b, Wernli et al. 2009) combined with accurate quantum reactive calculations. The quantum methods range from the fully ab-initio coupled channels (Bovino et al. 2009) to the use of a negative imaginary potential approach (Bovino et al. 2010a, 2010b) for the ionic systems. The computed reaction probabilities and cross sections have been reported in previous papers and we shall not repeat here the details of the calculations. The final state-to-all cross section obtained from the probability $(P_{a\to all}^J)$ is expressed as

$$\sigma_{(a\to all)}(E) = \frac{\pi}{(2j_a+1)k_a^2} \sum_{J} (2J+1)P_{a\to all}^J,$$
 (5)

where E is the collisional energy, j_a the molecular rotational angular momentum, J the total angular momentum, and k_a^2 is the wave vector defined as

$$k_a^2 = \frac{2\mu}{\hbar^2} (E - \varepsilon_a),\tag{6}$$

and ε_a is the a-channel energy. Rate coefficients are computed by averaging the appropriate reactive cross sections over a Boltzmann distribution of velocities for the incoming atom:

$$k(T_{\rm g}) = \frac{(8k_B T_{\rm g}/\pi\mu)^{1/2}}{(k_B T_{\rm g})^2} \int_0^\infty \sigma_{a\to all}(E) \exp(-E/k_B T_{\rm g}) E \, dE$$
 (7)

where T_g is the gas temperature, k_B is the Boltzmann constant and μ the reduced mass of the system. The newly computed rate coefficients for reactions (1), (2) and (3) are reported in Bovino et al. (2009, 2010a, 2010b) and shown in Figure 1. The corresponding temperature-dependent fits are given in Table 1, along with all the reactions rates for the Li species employed in the present work.

3. The chemical network and the evolutionary modelling

The evolution of the pregalactic gas is considered in the framework of a Friedmann cosmological model and the primordial abundances of the main gas components are taken from the standard big bang nucleosynthesis results (Smith et al. 1993). The numerical values of the cosmological parameters used in the calculation are obtained from WMAP5 data (Komatsu et al. 2009) and are listed in Table 2.

In order to calculate the abundances of LiH and LiH⁺, a set of differential coupled chemical rate equations of the form:

$$\frac{dn_i}{dt} = k_{\text{form}} n_j n_k - k_{\text{dest}} n_i + \dots$$
 (8)

has been solved. In eq. (8), k_{form} and k_{dest} are the formation and destruction reaction rates as listed in Table 1, and n_i is the number density of the reactant species i. The evolution of the gas temperature T_{g} is governed by the equation (see e.g. GP98):

$$\frac{dT_{\rm g}}{dt} = -2T_{\rm g}\frac{\dot{R}}{R} + \frac{2}{3kn}[(\Gamma - \Lambda)_{\rm Compton} + (\Gamma - \Lambda)_{\rm mol}],\tag{9}$$

where the first term represents the adiabatic cooling associated with the expansion of the Universe, R being the scale factor. The other two terms represent, respectively, the net transfer of energy from the CBR to the gas (per unit time and unit volume) via Compton scattering of CBR photons and electrons,

$$(\Gamma - \Lambda)_{\text{Compton}} = n_e \frac{4k\sigma_T a T_{\text{r}}^4 (T_{\text{r}} - T_{\text{g}})}{m_e c},$$
(10)

and via excitation and de-excitation of molecular transition

$$(\Gamma - \Lambda)_{\text{mol}} = \sum_{k} n_k \sum_{i>j} (x_i C_{ij} - x_j C_{ji}) h \nu_{ij}, \tag{11}$$

where C_{ij} and C_{ji} are the collisional excitation and de-excitation coefficients and x_i are the fractional level populations: for more details of this model see BG97 and GP98. The radiation temperature is $T_{\rm r}(z) = T_0(1+z)$, where T_0 is the present-day CBR temperature. The chemical/thermal network is then completed by the rate equation for the redshift

$$\frac{dt}{dz} = -\frac{1}{(1+z)H(z)},\tag{12}$$

where

$$H(z) = H_0 \sqrt{\Omega_{\rm r}(1+z)^4 + \Omega_{\rm m}(1+z)^3 + \Omega_{\rm K}(1+z)^2 + \Omega_{\Lambda}}.$$
 (13)

Here, H_0 is the Hubble constant and Ω_r , Ω_m , Ω_K , Ω_Λ are density parameters. The density n(z) of baryons at redshift z is

$$n(z) = \Omega_{\rm b} n_{\rm cr} (1+z)^3, \tag{14}$$

with $n_{\rm cr} = 3H_0^2/(8\pi G m_{\rm H})$ being the critical density. The calculations have been carried out from $z = 10^4$ down to z = 1 and are discussed in the next Section.

4. Results and discussion

As discussed in the Introduction, one of the novelties of the present work is the use, for some of the most important chemical processes, of rates obtained from accurate quantum calculations and not from qualitative estimates. It is therefore important for the reactions involving LiH/LiH⁺ to recall the behavior of the ab-initio reactive rates (in the temperature range of interest) that have been obtained via the quantum methods outlined in Section 2. The data reported in Figure 1 indicate the depletion rates for the disappearance of LiH molecules by exothermically reacting with the surrounding atomic hydrogen (top panel). The temperature behavior of the ab-initio data is clearly very different from that assumed by SLD96. The new calculations of Bovino et al. (2009) indicate a variation over the same range of nearly three orders of magnitude. The same occurs for the destruction reaction of LiH by interaction with protons (middle panel): the ab-initio calculations (Bovino et al. 2010b) show that the rate varies by about one order of magnitude over the same range of temperatures. Finally, the quantum rates associated with the destruction of LiH⁺ by the surrounding hydrogen gas (bottom panel) confirm the weak temperature dependence reported earlier (Lepp et al. 2002), although they turn out to be about a factor of 4 larger than the estimate of SLD96. Once the new quantities are employed within the evolutionary scheme outlined in Section 3, they yield a new set of production/destruction rates of LiH and LiH⁺ as a function of redshift, as shown in Figure 2 and 3.

4.1. LiH chemistry

The various curves shown in Figure 2 follow the notation given in Table 1 to the most relevant processes: those labelled as p_1, \ldots, p_4 (solid lines) refer to the different reactions leading to LiH production, while those labelled d_1, \ldots, d_4 (dashed lines) refer to the destruction processes. A look at the figure allows one to make the following comments:

- (i) The production by radiative recombination from the $\text{Li}(^2P)$ state (p_1) clearly dominates at high redshifts, while the production by recombination from the $\text{Li}(^2S)$ state (p_2) becomes the dominant route from $z \simeq 800$ down to $z \simeq 80$. Then, the channel of recombination driven by electron attachment (p_4) takes over. However, we must note that the latter rate is not known from quantum calculations, but only estimated by SLD96, together with the estimates of LiH formation from H⁻ (SLD96).
- (ii) At the highest redshifts, the destruction channel is dominated by photodissociation (d_1) , a rate estimated from the detailed balance of process (p_2) , while at lower z values $(z \lesssim 300)$ the collisional process of reactive destruction discussed earlier (d_2) takes over and dominates the whole destruction channel down to the lowest redshifts. The same reactive process with protons (d_3) is seen to be less important, although larger than previous estimates (d_4) .

In conclusion, the above data indicate that the radiative photoassociation from the n = 25 level of Li is the most significant formation path, while the collisional destruction by H (d_2) overcomes production over the whole range of redshifts below 300.

4.2. LiH $^+$ chemistry

Figure 3 shows the processes leading to the formation and the destruction of LiH⁺, labelled as p_1^+, \ldots, p_2^+ and d_1^+, \ldots, d_4^+ as in Table 1. As clearly shown by the figure, the radiative association processes $(p_1^+ \text{ and } p_2^+)$ are seen to dominate the formation of LiH⁺ over a very broad range of redshifts. The association involving the Li ion (p_1^+) is the major pathway down to about $z \simeq 700$, when the reaction of H⁺ with neutral Li (p_2^+) takes over and becomes dominant by several orders of magnitude over the rates of the charge-exchange reaction (p_3^+) estimated by SLD96.

As for the destruction processes for LiH⁺, one sees that photodissociation (d_1^+) is the dominant destruction path of the ionic molecule, due to its small dissociation energy value. Furthermore, the dominant dissociation channel comes from Li⁺ production (d_3^+) , while the one yielding H⁺ (d_2^+) is relevant only at the highest redshifts. The electron-induced dissociation (d_4^+) was earlier based on a simple estimates from SLD96 while now we have included the more accurate quantum calculations from Čurik & Greene (2007,2008) which yield much larger rates. It turns out to be important only at low redshifts. On the other hand, the chemical paths which involve the reactions that destroy LiH⁺ (d_3^+) are seen to be indeed the most important processes around $z \simeq 40$ while becoming less efficient than the d_4^+ process below $z \simeq 10$. The electron-assisted dissociation of LiH⁺ (d_4^+) is therefore important only at the lowest redshifts.

In summary, the ionic formation is dominated by the radiative association of Li with H⁺ over a very broad range of redshifts, while destruction by photodissociation prevails at larger redshift and chemical destruction (d_3^+) dominates at lower redshifts. However, down to $z \simeq 1$ the dissociative neutralization (d_4^+) is markedly dominant.

4.3. Chemical evolution

The new evolution of relative abundances of atomic and molecular species involving Li is displayed in Figure 4, comparing the earlier results obtained with the chemical network of GP98 (dashed lines) and the present results (solid lines) which employ the new quantum rates. The main results are the following:

- (i) The temperature dependence of the quantum rates, shown by the data of Figure 1, is clearly reflected in the molecular abundances of LiH at redshifts below $z \sim 300$. The rapid rise of LiH at $z \sim 300$ found by GP98 is no longer seen owing to the increased destruction rate of channel (1). The rise at $z \sim 100$ is due to the importance of LiH formation by Li⁻ that persists at all redshifts together with the radiative association of Li with H. This is drastically different from the behavior found by GP98 where the constant value of the rate for reaction (1) caused the steady drop of LiH. The final (z = 0) value of LiH is $\sim 7 \times 10^{-18}$ with an increase of a factor of ~ 70 relative to GP98.
- (ii) Due to the differences in behavior shown by the cross sections in Figure 1, the ionic partner, LiH^+ , behaves differently at $z \lesssim 30$. First, the increased efficiency of LiH^+ destruction (reaction 3;

rate d_3^+) limits the sharp rise in abundance at $z \sim 20$. Then, the gentle decline below $z \sim 5$ is due to the efficiency of electronic recombination (rate d_4^+). The new final abundances of LiH⁺ (solid line) is now smaller than earlier estimates of GP98 by a factor of ~ 20 .

The scenario emerging from the above calculations therefore indicates that in the regions of redshift below $z \simeq 30$, LiH remains the more abundant species compared to LiH⁺, but only by a factor of $\sim 2-7$. The two molecular abundances, on the other hand, reach the largest values for $z \lesssim 10$, remaining both fairly small (LiH $\sim 10^{-17}$, LiH⁺ $\sim 10^{-18}$) and hard to detect.

5. Conclusions

Building upon recent quantum reactive calculations (Bovino et al. 2009, 2010a, 2010b) involving the chemical evolution of LiH/LiH⁺ molecules within the expected conditions in the early universe, the present work has revisited the analysis of all the dynamical processes that are known to significantly contribute to the production/destruction of the lithium-containing molecules. We have employed as many results as possible from calculations based on ab-initio methods, both for the interaction forces and the quantum dynamics, resorting to estimates only for a few of the considered processes.

One of the main results from the quantum reactive calculations is that two of the important rates exhibit a temperature dependence that was not present in the earlier estimates.

The results for the abundance of LiH indicate that this molecule is now much more likely to have survived at low redshift, since its fractional abundance, albeit still fairly small, goes up by a factor of ~ 70 compared to previous estimates. However, it becomes smaller by nearly the same amount for z > 300.

The fractional abundance of LiH⁺ only becomes significant in the low-redshift region of $z \lesssim 30$ and shows a reduced value of the relative abundance by about one order of magnitude with respect to the earlier estimates. The comparison between the specific fractional abundances of the two species now indicates that the neutral molecule is likely to be more abundant than the ionic species and that their ratio in the region of small redshift increases up to a factor of 7 down to $z \simeq 1$. Unlike previous estimates that predicted a difference at low-z of about two orders of magnitude in favor of LiH⁺, the new calculations find more comparable abundances of LiH and LiH⁺. Furthermore, we find that the neutral molecule, in spite of a large dilution at the low redshifts, should be more amenable to experimental observation (e.g., Persson et al. 2010) than its ionic counterpart.

Finally, given the recent studies (e.g. see Zaldagarriaga and Loeb, 2002) on the possible detection, wihin the microwave background anisotropies, of the earlier imprint from the recombination history of lithium, the present results strongly suggest that such anisotropies could be amenable to observation due to the changed optical depth induced by the changes on lithium abundances

Acknowledgments We thank the CINECA and CASPUR consortia for providing us with the necessary computational facilities and the University of Roma "Sapienza" for partial financial support.

REFERENCES

Bennett O.J., Dickinson, A.S., Leininger, T., Gadéa, F.X. 2003, MNRAS, 341, 361

Bennett O. J., Dickinson A. S., Leininger T. & Gadéa F. X., 2008, MNRAS, 384, 1743

Bougleux E. & Galli D., 1997, MNRAS., 288, 638 (BG97)

Bovino S., Wernli M. & Gianturco F. A., 2009, ApJ, 699, 383

Bovino S., Stoecklin T. & Gianturco F. A., 2010a, ApJ, 708, 1560

Bovino S., Tacconi M., Gianturco F. A. & Stoecklin T., 2010b, ApJ, 724, 106

Bulut N., Castillo J. F., Aoiz F. J., & Banares L., 2008, Phys. Chem. Chem. Phys., 10, 821

Cyburt R. M., Fields B. D. & Olive K. A., 2008, J. Cosmol. Astropart. Phys., 11, 12

Croft H., Dickinson A. S. & Gadéa F. X., 1999, MNRAS, 304, 327

Curík R. & Greene C. H., 2007, Phys. Rev. Lett., 98, 173201

Curík R. & Greene C. H., 2008, J. Phys.: Conference Series, 115, 012016

Dalgarno A., Kirby K. & Stancil P. C., 1996, ApJ, 458, 397

Defazio P., Petrongolo C., Gamallo P. & González M., 2005, J. Chem. Phys., 122, 214303

Dubrovich V. K., 1993, Astron. Lett., 19, 53

Dunne L. J., Murrell J. N. & Jemmer P., 2001, Chem. Phys. Lett., 336, 1

Galli D., Palla F., 1998, A&A, 335, 403 (GP98)

Gianturco F. A. & Gori Giorgi P., 1996, Phys. Rev. A., 54, 1

Gianturco F. A. & Gori Giorgi P., 1997, ApJ, 479, 560

Kimura M., Dutta C. M. & Shimakura N., 1994, ApJ, 430, 435

Komatsu, E., et al. 2009, ApJS, 180, 330

Lepp, S. & Shull, J.M. 1983, ApJ, 270, 578

Lepp S., Stancil P. C. & Dalgarno A., 2002, J. Phys. B:At. Mol. Opt. Phys., 35, R57-R80

Maoli R., Melchiorri F., and Tosti D., 1994, ApJ, 425, 372

Martinazzo R., Bodo E., Gianturco F. A., & Raimondi M., 2003a, Chem. Phys., 287, 335

Martinazzo R., Tantardini G. F., Bodo E., & Gianturco F. A., 2003b, J. Chem. Phys., 119, 11241

Peebles P. J. E., 1993, Principles of Physical Cosmology, Princeton University Press, Princeton

Persson, C. M., et al. 2010, A&A, 515, A72

Pino I., Martinazzo R., & Tantardini G., 2008, Phys. Chem. Chem. Phys., 10, 5545

Ramsbottom C. A., Bell K. L. & Berrington K. A., 1994, J. Phys. B, 27, 2905

Smith M. S., Kawano L. H. & Malaney R. A., 1993, ApJS, 85, 219

Schleicher, D. R. G., Galli, D., Palla, F., Camenzind, M., Klessen, R. S., Bartelmann, M., & Glover, S. C. O. 2008, A&A, 490, 521

Spergel D. N., et al. 2007, ApJS, 170, 377

Stancil P. C., Lepp S. & Dalgarno A., 1996, ApJ, 458, 401 (SLD96)

Stancil P. C. & Zygelman B., 1996, ApJ, 472, 102

Verner D. A., Ferland G. J., 1996, ApJS, 103, 467

Vonlanthen, P., Rauscher, T., Winteler, C., Puy, D., Signore, M., Dubrovich, V. 2009, A&A, 503, 47

Wagoner R. V., Fowler W. A. & Hoyle F., 1967, ApJ, 148, 3

Wernli M., Caruso D., Bodo E. & Gianturco F. A., 2009, J. Phys. Chem. A., 113, 1121

Zaldagarriaga M., & Loeb A., 2002, ApJ, 564, 52

Table 1: List of considered reactions. Labels in the second column refer to Figures 2 and 3.

| | | reaction | rate (cm 3 s $^{-1}$ or s $^{-1}$) | notes | reference |
|-----|------------------|--|---|---|-------------|
| | | | Li reactions | | |
| 1) | p_1 | $\text{Li}(^2p) + \text{H} \rightarrow \text{LiH} + h\nu$ | $2.0 \times 10^{-16} T_{\rm g}^{0.18} \exp(-T_{\rm g}/5100)$ $1.9 \times 10^{-14} T_{\rm g}^{-0.34}$ | $A^1\Sigma^+ \to X^1\Sigma^+$, quantal calc. | (a) |
| 2) | p_1 | $\operatorname{Li}(^2p) + \operatorname{H} \to \operatorname{LiH} + h\nu$ | $1.9 \times 10^{-14} T_{\rm g}^{\rm g}$ | $B^1\Pi \to X^1\Sigma^+$, quantal calc. | (a) |
| 3) | p_2 | $\text{Li} + \text{H} \rightarrow \text{LiH} + h\nu$ | $4.0 \times 10^{-20} \times^{g}$ | | |
| | | | $\exp[-T_{\rm g}/4065 + (T_{\rm g}/13193)^3]$ | quantal calc. | (b),(c),(d) |
| 4) | p_3 | $Li + H^- \rightarrow LiH + e$ | 4.0×10^{-10} | estimate | (e) |
| 5) | p_2^+ | $\text{Li} + \text{H}^+ \rightarrow \text{LiH}^+ + h\nu$ | $5.3 \times 10^{-14} T_{\rm g}^{-0.49}$ | quantal calc. | (c),(d) |
| 6) | | $Li + H^+ \rightarrow Li^+ + H$ | $2.5 \times 10^{-40} T_{g}^{\text{ff.9}} \exp(-T_{g}/1210)$ $1.7 \times 10^{-13} T_{g}^{-0.051} \exp(-T_{g}/282000)$ | quantal calc. | (f) |
| 7) | | $Li + H^+ \rightarrow Li^+ + H + h\nu$ | $1.7 \times 10^{-13} T_{\rm g}^{-0.051} \exp(-T_{\rm g}/282000)$ | quantal calc. | (g) |
| 8) | | $\text{Li} + \text{e} \rightarrow \text{Li}^- + h\nu$ | $\begin{array}{l} 6.1 \times 10^{-17} T_0^{0.58} \exp(-T_g/17200) \\ 6.3 \times 10^{-10} \exp(-2553/T_g) \\ 7.2 \times 10^{-14} T_g^{1.18} \exp(-1470/T_g) \end{array}$ | det. bal. applied to (27) | |
| 9) | | $Li + H_2^+ \rightarrow LiH + H^+$ | $6.3 \times 10^{-10} \exp(-2553/T_{\rm g})$ | $T_{\rm g}$ < 500, quantal calc. | (i) |
| | | | $7.2 \times 10^{-14} T_{\rm g}^{1.18} \exp(-1470/T_{\rm g})$ | $T_{\rm g} > 500$, quantal calc. | (j) |
| | | | Li ⁺ reactions | | |
| 10) | p_1^+ | $Li^+ + H \rightarrow LiH^+ + h\nu$ | $1.4 \times 10^{-20} T_{\rm g}^{-0.9} \exp(-T_{\rm g}/7000)$ | quantal calc. | (c),(d) |
| 11) | | $Li^+ + e \rightarrow Li + h\nu$ | $\begin{array}{l} 1.036 \times 10^{-11} [\sqrt{T_{\rm g}/107.7} \times \\ (1+\sqrt{T_{\rm g}/107.7})^{0.6612} \times \end{array}$ | | |
| | | | $(1+\sqrt{T_{\rm g}/107.7})^{0.6612} \times$ | | |
| | | | $(1+\sqrt{T_{\rm g}/1.177\times10^7})^{1.3388}]^{-1}$ | quantal calc. | (k) |
| 12) | | $Li^+ + H^- \rightarrow Li + H$ | $6.3 \times 10^{-9} T_{\rm g}^{-1/2} (1 + T_{\rm g}/14000)$ | Landau-Zener approx. | (1) |
| | | | Li ⁻ reactions | | |
| 13) | p_4 | $Li^- + H \rightarrow LiH + e$ | 4.0×10^{-10} | estimate | (e) |
| 14) | | $Li^- + H^+ \rightarrow Li + H$ | $2.3 \times 10^{-6} T_{\rm g}^{-1/2}$ | Landau-Zener approx. | (1) |
| | | | LiH reactions | | |
| 15) | d_2 | ${\rm LiH}+{\rm H}\rightarrow{\rm Li}+{\rm H}_2$ | $2.0 \times 10^{-12} T_{\rm g} \exp(-T_{\rm g}/1200)$ | quantal calc. | (m) |
| 16) | d_3 | $LiH + H^+ \rightarrow Li + H_2^+$ | $2.9 \times 10^{-10} T_{\sigma}^{0.59}$ | | |
| | | | $-2.6 \times 10^{-10} T_{\rm g}^{\rm 0.60} \exp(-400/T_{\rm g})$ | quantal calc. | (n) |
| 17) | p_3^+, d_4 | $LiH + H^+ \rightarrow LiH^+ + H$ | 1.0×10^{-9} | quantal calc. | (o) |
| 18) | d_4 | $LiH + H^+ \rightarrow Li^+ + H_2$ | 1.0×10^{-9} | estimate | (e) |
| | | | LiH ⁺ reactions | | |
| 19) | d_3^+ | $LiH^+ + H \rightarrow Li^+ + H_2$ | $8.7 \times 10^{-10} T_{\rm g}^{0.040} \exp(T_{\rm g}/5.92 \times 10^8)$ | quantal calc. | (p) |
| 20) | d_3^+ | $LiH^+ + H \rightarrow Li + H_2^+$ $LiH^+ + H \rightarrow LiH + H^+$ | $9.0 \times 10^{-10} \exp(-66400/T_g)$ | estimate | (e) |
| 21) | d_3^{\uparrow} | $LiH^+ + H \rightarrow LiH + H^+$ | $1.0 \times 10^{-11} \exp(-67900/T_{\rm g})$ | estimate | (e) |
| 22) | d_4^+ | $LiH^+ + e \rightarrow Li + H$ | $3.9 \times 10^{-6} T_{\rm g}^{-0.70} \exp(-T_{\rm g}/1200)$ | quantal calc. | (p) |
| | | | photoreactions | | |
| 23) | d_1 | $LiH + h\nu \rightarrow Li + H$ | | det. bal. applied to (3) | |
| 24) | d_1^+ | $LiH^+ + h\nu \rightarrow Li^+ + H$ | | det. bal. applied to (10) | |
| 25) | d_2^{\uparrow} | $LiH^+ + h\nu \rightarrow Li + H^+$ | | det. bal. applied to (5) | |
| 26) | | $\text{Li} + h\nu \rightarrow \text{Li}^+ + \text{e}$ | | det. bal. applied to (11) | (1.) |
| 27) | | $\text{Li}^- + h\nu \to \text{Li} + \text{e}$ $\text{LiH} + h\nu \to \text{Li}(^2p) + \text{H}$ | | quantal calc. | (h) |
| 28) | | $Lin + n\nu \rightarrow Li(-p) + H$ | | det. bal. applied to (1) , (2) | |

⁽a) Gianturco & Gori Giorgi (1996); (b) Bennett et al. (2003, 2008); (c) Dalgarno, Kirby & Stancil (1996); (d) Gianturco & Gori Giorgi (1997); (e) Stancil, Lepp & Dalgarno (1996); (f) Kimura, Dutta & Shimakura (1994); (g) Stancil & Zygelman (1996); (h) Ramsbottom, Bell & Berrington (1994); (i) Bulut et al. (2009); (j) Pino et al. (2008); (k) Verner & Ferland (1996); (l) Croft, Dickinson & Gadéa (1999); (m) Bovino, Wernli & Gianturco (2009); (n) Bovino et al. (2010); (o) Bulut et al. (2008); (p) Bovino, Stoecklin & Gianturco (2010); (q) Čurik & Greene (2007, 2008).

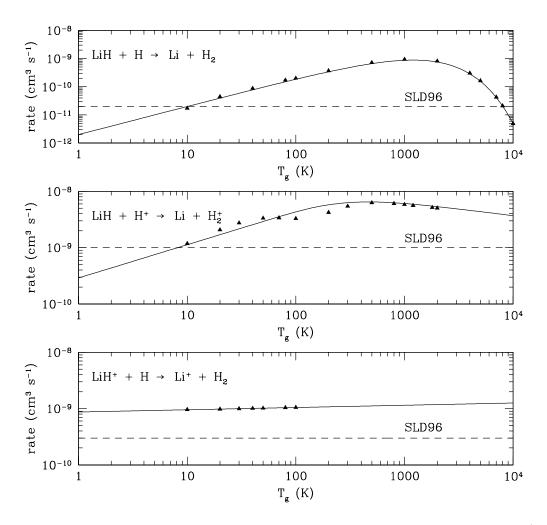


Fig. 1.— A comparison of reaction rates for: destruction of LiH with H reaction (top panel) and H⁺ (middle panel); destruction of LiH⁺ with H (lower panel). The solid lines are fits of the computed data (open triangles) which used quantum reactive scattering methods (see Section 2). Dashed curved represent estimates by SLD96.

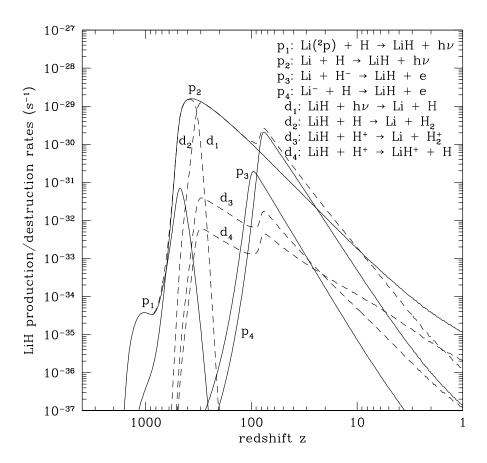


Fig. 2.— Computed production/destruction rates of LiH as function of redshift. Solid and dashed curves represent production and destruction processes, respectively. See text for details.

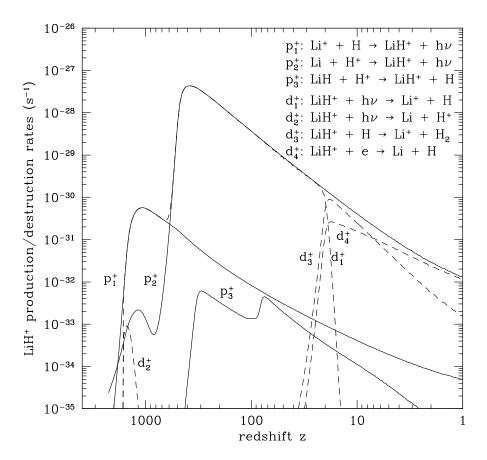


Fig. 3.— Same as Figure 2 for LiH⁺. See text for details.

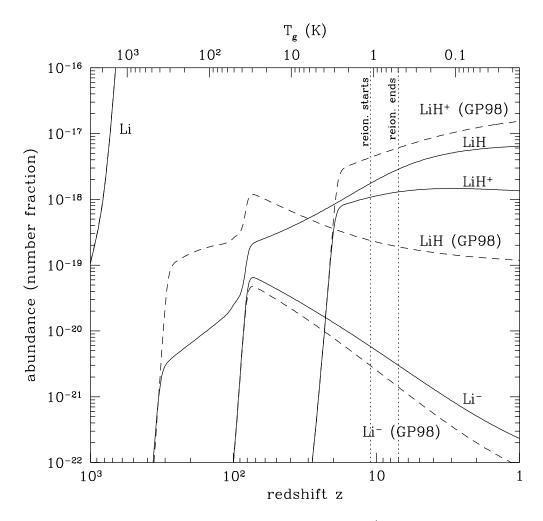


Fig. 4.— Relative abundances of Li, Li⁻, LiH, and LiH⁺ in the post-recombination era as function of redshift z (lower scale) and gast temperature $T_{\rm g}$ (upper scale): present results (solid curves), results of GP98 (dashed curves). The dotted lines at $z{=}11$ and z=7 indicate the approximate redshifts at which reionization of the primordial gas starts ($z\simeq11$) and is completed ($z\simeq7$), according to Spergel et al. (2007).

Table 2: Cosmological model

| Table 2: Cosmological model | | | |
|-----------------------------|--|--|--|
| Parameter | Numerical value | | |
| H_0 | $70.5 \text{ km s}^{-1} \text{ Mpc}^{-1}$ | | |
| T_0 | $2.725~\mathrm{K}$ | | |
| $z_{ m eq}$ | 3141 | | |
| $\Omega_{ m dm}$ | 0.228 | | |
| $\Omega_{ m b}$ | 0.0456 | | |
| $\Omega_{ m m}$ | $\Omega_{ m dm} + \Omega_{ m b}$ | | |
| $\Omega_{ m r}$ | $\Omega_m/(1+z_{ m eq})$ | | |
| Ω_{Λ} | 0.726 | | |
| $\Omega_{ m K}$ | $1-\Omega_{\rm r}-\Omega_{\rm m}-\Omega_{\Lambda}$ | | |
| $f_{ m H}$ | 0.924 | | |
| $f_{ m He}$ | 0.076 | | |
| $f_{ m D}$ | 2.38×10^{-5} | | |
| $f_{ m Li}$ | 4.04×10^{-10} | | |